water

MDPI

Article

Kinetic Analysis of Rainfall-Induced Landslides in May 2022 in Wuping, Fujian, SE China

Tao Wang [1,2,3], Ran Li [1,2,*], Cheng Chen [1,3,*], Jiangkun He [4], Chenyuan Zhang [4], Shuai Zhang [1,2,3], Longzhen Ye [3], Kan Liu [3] and Kounghoon Nam [5]

1 Institute of Geomechanics, Chinese Academy of Geological Sciences, Beijing 100081, China
2 Observation and Research Station of Geological Disaster in Baoji, Shaanxi Province, Ministry of Natural Resources, Baoji 721001, China
3 Key Laboratory of Geohazard Prevention of Hilly Mountains, Ministry of Land and Resources (Fujian Key Laboratory of Geohazard Prevention), Fuzhou 350002, China
4 Faculty of Geosciences and Environmental Engineering, Southwest Jiaotong University, Chengdu 611756, China
5 Department of Earth and Environmental Sciences, Andong National University, Andong 1375, Republic of Korea
* Correspondence: 13261553306@163.com (R.L.); 13001281336@163.com (C.C.); Tel.: +86-10-8881-5062 (R.L.)

Abstract: In the context of global climate change, shallow landslides induced by strong typhoons and the ensuing rainstorms have increased significantly in China's eastern coastal areas. On 27 May 2022, more than 700 liquefied landslides were induced by the rain gush in Wuping County, Longyan City, Fujian Province, SE China. In light of their widespread occurrence and the severe damage caused, detailed field investigations, UAV surveys, trench observations, in situ tests, and numerical simulation are conducted in this work. The cascading landslides are classified as channelized landslides and hillslope landslides. Long-term rainfall, the influence of vegetation roots under wind load, and differences in the strength and structure of surficial soil are the dominant controlling factors. The sliding surface is localized to be the interface at a depth of 1–1.5 m between the fully weathered granite and the strongly weathered granite. Kinetic analysis of a channelized landslide shows that it is characterized by short runout, rapid velocity, and strong impact energy. The maximum velocity, impact energy, and impact force of the Laifu landslide are 29 m/s, 4221.35 J, and 2110 kPa. Effective excavation is usually impossible in this context. This work highlights the escalating issue of shallow landslides in eastern China's coastal areas, exacerbated by climate change and extreme weather events like typhoons. By conducting comprehensive investigations and analyses, the research identifies key factors influencing landslide occurrence, such as rainfall patterns and soil characteristics. Understanding the dynamics and impact of these landslides is vital for improving risk assessment, developing effective early warning systems, and informing land management policies in this region. Further exploration concerning hydro-meteorological hazard early warning should be encouraged in this region.

Keywords: typhoon rainstorm; rainfall-induced landslide; weathered granite; failure mechanism; kinetic analysis

check for updates

Citation: Wang, T.; Li, R.; Chen, C.; He, J.; Zhang, C.; Zhang, S.; Ye, L.; Liu, K.; Nam, K. Kinetic Analysis of Rainfall-Induced Landslides in May 2022 in Wuping, Fujian, SE China. *Water* **2024**, *16*, 3018. https://doi.org/10.3390/w16213018

Academic Editor: Roberto Gaudio

Received: 7 September 2024
Revised: 8 October 2024
Accepted: 12 October 2024
Published: 22 October 2024

Copyright: © 2024 by the authors. Licensee MDPI, Basel, Switzerland. This article is an open access article distributed under the terms and conditions of the Creative Commons Attribution (CC BY) license (https://creativecommons.org/licenses/by/4.0/).

1. Introduction

In the 21st century, the global climate has changed dramatically, and the frequency of extreme events (such as typhoons) has gradually increased, posing a serious threat to the safety of lives and property. Landslides triggered by typhoons and the ensuing torrential precipitation pose a catastrophic threat to many countries in the northwest Pacific. China is one of the few countries in the world most affected by typhoons [1,2], especially in the southeastern coastal areas. The southeastern coastal area of China belongs to the subtropical monsoon climate and this area is warm and humid with abundant rainfall and

strong physical rock weathering. The slope surface is mostly covered by residual soil and strongly weathered rocks. The structure is loose, and cracks are well developed, making it extremely prone to various types of geological disasters [3,4]. In this light, rainfall-induced landslides in the eastern coastal areas of China occur almost every year. On 10 August 2019, a cascade of landslides caused by extremely heavy rains in Zhejiang Province during super typhoon "Lekima" caused 71 deaths and $9.3 billion in losses [5]. In May 2019, more than 170 shallow landslides were triggered by heavy rainfall in Sanming City, Fujian Province, SE China [6]. In September 2010, massive shallow landslides were induced by heavy rainfall in a large region of Magui Town, Guangdong Province [7]. Considerable investigations have been conducted on cluster rainfall-induced landslides in previous work, including regional-scale susceptibility assessments [8–12] and single-scale instability simulations and motion process simulations based on onsite monitoring or physical model tests [13–18]. However, there are relatively few studies on the movement process of rainstorm-induced landslides, especially the impact of such landslides on buildings at the foot of the slope.

The southeastern coastal regions of China are annually threatened by typhoon landfalls, which bring intense rainfall and destructive storm surges, leading to numerous shallow landslides and debris flows that directly impact millions of people. The increasing frequency of extreme precipitation events in recent years has led to a rise in recorded catastrophic landslides [19], such as the NiuShou landslide in Nanjing, Jiangsu Province, on 11 June 2016 [20]. Despite the close relationship between hydrological factors and rainfall-induced landslides, hydrological processes have received insufficient attention in landslide research over the past several decades [21]. Future studies should emphasize meteorological–hydrological–geological coupling processes. Some researchers have systematically outlined the mechanisms by which five primary meteorological factors—rainfall, temperature, humidity, wind, and solar radiation—affect slope stability, analyzing the interrelated effects of soil cracking, surface vegetation, and soil–atmosphere interactions. Proposed future research directions include the development of theoretical models for soil–vegetation–atmosphere interactions [22]. Numerical models have quantitatively assessed the impacts of wind loads, rainfall infiltration, and root reinforcement on slope stability, with findings compared to cases from Huapai'a and Whairoa in New Zealand. Results indicate that the influence of trees on slope stability during typhoons varies due to differences in meteorological conditions and soil thickness; while they negatively affect slope stability in southeastern China, they enhance stability in New Zealand. Landslides triggered by typhoons in southeastern China result from the combined effects of wind, vegetation, and rainfall, suggesting that uniform infiltration alone is insufficient to explain the landslide mechanisms during typhoons. The interaction of wind loads and dominant infiltration effects at the root–soil interface significantly impacts stability [23]. Numerous studies have focused on the large-scale shallow landslide event in the MaGui Town watershed on 21 September 2010, revealing that mass shallow landslides were concentrated in areas with developed vegetation, while sparsely vegetated regions experienced few occurrences. Using the double-ring method, researchers measured the initial and steady-state infiltration rates of granite residual soils across three vegetated areas. By introducing the macropore coefficient of granite residual soil, they investigated the hydrological effects of macropore flow, integrating hydrological and shallow landslide models to calculate rainfall thresholds for slope units, achieving a model prediction accuracy of 80.65% [7]. However, research on the kinematic characteristics of extreme-rainfall-induced geological disasters in the southeastern coastal regions remains limited, particularly concerning the dynamic evolution of mass-rainfall-induced landslide events. This work focuses on typical geological disasters triggered by extreme rainfall in Fujian Province, SE China. By employing methods such as field investigations, in situ testing, UAV surveys, and numerical simulations, the study aims to elucidate the dynamic evolution and movement impact characteristics of these landslide disasters.

2. Study Area

Fujian Province is a typical typhoon and rainstorm-affected area in the southeastern coastal area of China and is also one of the major landslide-prone areas in China [24]. Residual soil layers and weathered granite layers are widely distributed, and rock fissures, fault joints, and weak structural surfaces are well developed in SE China [25,26]. Landslides have long been a major concern in SE China [27]. In May 2022, rainstorms in Longyan City, Fujian Province induced 707 shallow landslides (Figure 1) and caused serious losses of life, property, and road operations. At around 3:30 a.m. on 27 May 2022, the slope near Laifu Village, Shifang Town, Longyan City, Fujian Province suddenly became unstable, and a landslide occurred, killing a total of five people and destroying some buildings. Then, at around 5:00 a.m., a landslide occurred near Zhongdi Natural Village, Shifang Town, Longyan City, Fujian Province, causing a total of three deaths. Studying the development characteristics and kinematic mechanisms of this type of landslide is of guiding significance for the early warning and emergency response to landslides. Based on field measurements, aerial photogrammetry, and numerical simulations, this paper takes the Laifu landslide as an example to analyze the effects of typhoon rainstorms in Fujian Province. A preliminary study was conducted on the failure mechanism and kinematic characteristics of shallow landslides triggered by rainstorms in an area widely mantled by highly weathered igneous rock.

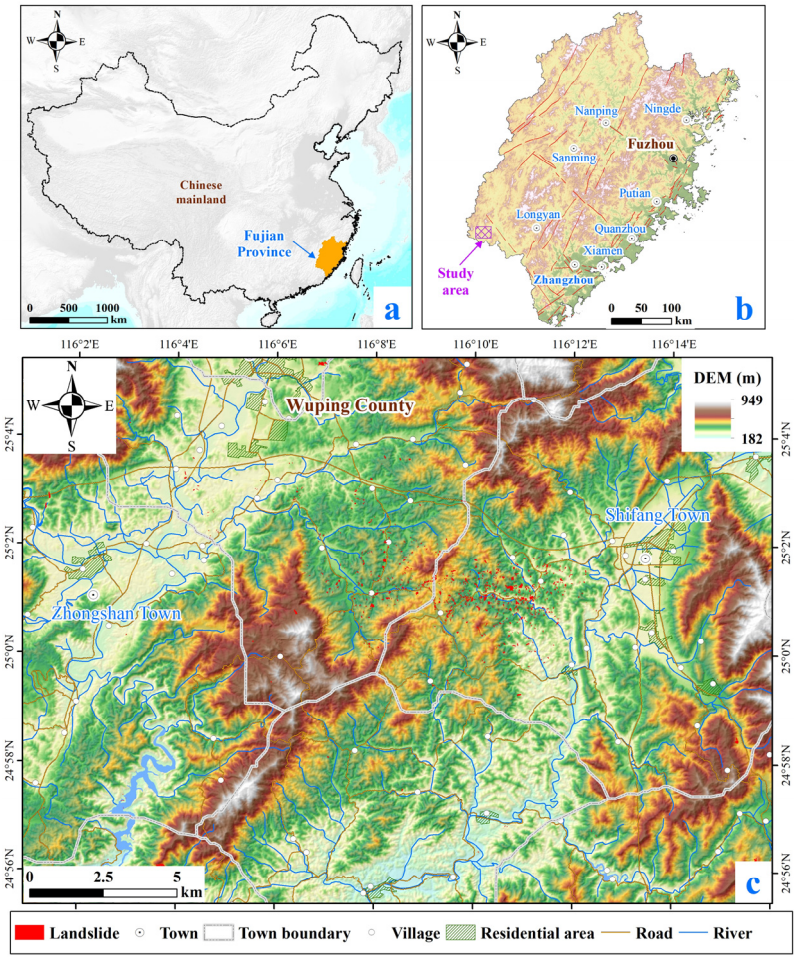


Figure 1. Location map of cascading landslides induced by the rain gush on 27 May 2022 in SE China. (**a**) Location of Fujian province. (**b**) Location of the study area. (**c**) Landslide inventory map.

The study area is located in Wuping County, Longyan City, Fujian Province, Southeast China (Figure 1). This region belongs to the Longyan Basin and features an east–west

neocathaysian structural system. The study area, with a total area of about 485 km^2, is featured by low hills. Hills, valleys, and flat areas are staggered in this region. The landform belongs to the wind-erosion monadnock with lush vegetation. The groundwater is mainly composed of Quaternary phreatic water and bedrock fissure water. The phreatic water mainly exists in the sandy clay on the residual slope and the loose weathered layer with a buried depth of more than 10 m. Bedrock fissure water exists in the weathered fissures of the underlying bedrock. The geological structure is complex, and faults are well developed (Figure 2). Strata of various geological eras are developed and exposed. The lithology is mainly tuff, mudstone, sandstone, limestone, dolomitic limestone, dolomite, phyllite, andesite, basalt, and granite (Figure 2). Quaternary sediments of various origins overlie impermeable bedrock. The surface soil layers of the slope are mainly composed of humus soil with a loose structure, clayey soil accumulated on the residual slope, and fully weathered granite. The lower part is strongly weathered granite with a dense structure and visible original rock structure, which is in the shape of broken pieces. The soil on the residual slope is easily saturated with overland flow and softened by rainfall, and its shear strength can be sharply reduced. It suffers slope failure easily under extreme rainfall conditions.

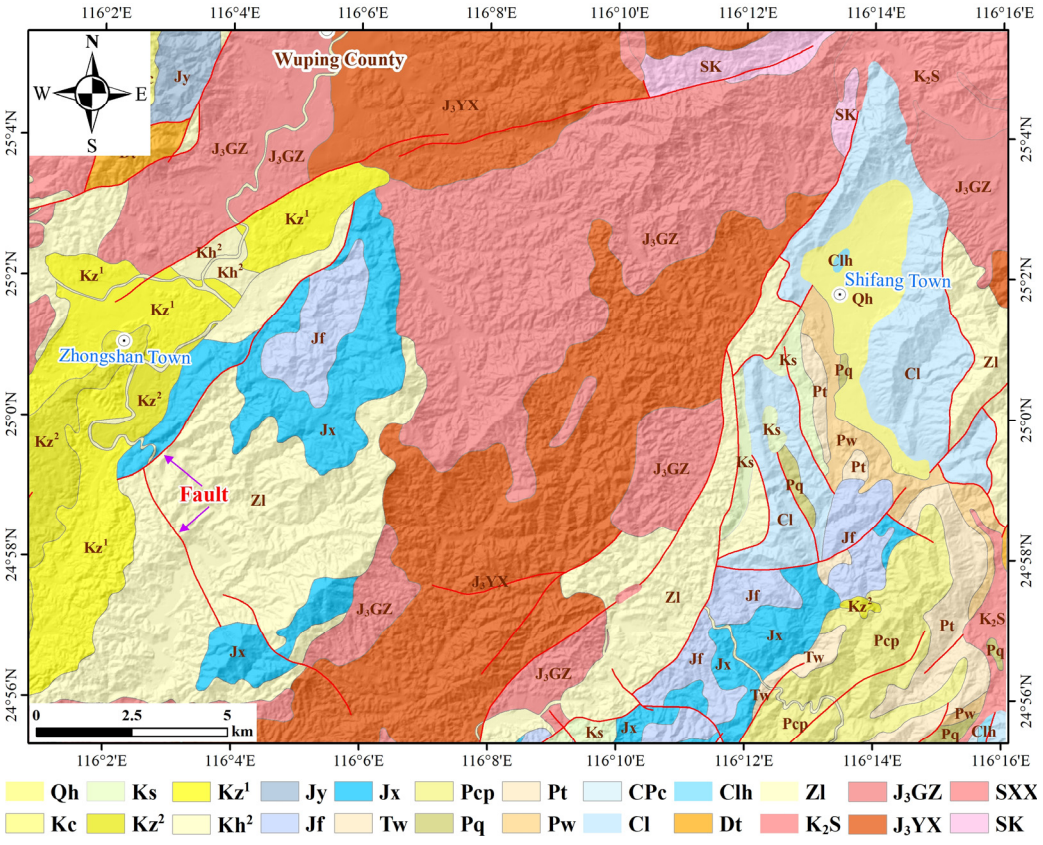


Figure 2. Geological setting of the study area.

In terms of climate, Longyan City is characterized by a subtropical maritime monsoon climate and the four seasons are well distinguished. Heavy rains are concentrated in summer and typhoons invade frequently in autumn, with local rainstorms being short in duration and strong in intensity. The multi-year average temperature is 19.1 °C, and the average annual rainfall is approximately 1500–1900 mm. Rainfall is usually concentrated from April to September, accounting for 80% of the annual rainfall, and the rainfall volume between May and June accounts for 36% of the annual rainfall. On 27 May 2022, torrential rainfall struck this region, and cascades of landslides were induced in the study area. Based

on our preliminary analysis, 707 landslides were triggered and serious property losses and casualties resulted due to the sharp increase in occurrence of the cascading landslides.

3. Typical Landslide

The cluster landslides induced by the heavy rainfall on 27 May 2022 in this region can be classified into hillslope landslides and channelized landslides. In light of the severe destruction resulting from the relatively long runout and high mobilization of the channelized landslides, a preliminary investigation including a field investigation, an unmanned aerial vehicle (UAV) survey, a trench observation, in situ tests, and a kinetic analysis were conducted on the Laifu landslide. The Laifu landslide was located at Laifu Village, Shifang Town, Longyan City, Fujian Province. Around 3:30 on 27 May 2022, the Laifu landslide suddenly occurred and destroyed the factory at the slope toe (Figure 3a). This slope failure resulted in five casualties. The Laifu landslide featured a flacon shape with a slip direction of approximately 234.2°. It initiated from an elevation of 339.7 m (Figure 3b) and rested at an elevation of approximately 281.5 m after destroying the factory (Figure 3c). The total area affected by the Laifu landslide is approximately 2224 m^2 and the sliding surface is approximately 0.5–1.5 m. The total volume of the sliding mass is estimated to be approximately 1600 m^3. The sliding mass mainly comprises sandy clay soil deposited on the residual slope. The sandy clay soil is weathered from the medium-coarse-grained granite and the quartz sand content is higher (Figure 3d). The sliding mass is featured by good permeability. Clear black weathering crusts can be observed on the slide surface, and strongly weathered granite underlies the weathering crust (Figure 3e). The medium-coarse-grained granite that was strongly weathered can be spotted at the main scarp (Figure 3f) and the original rock structure can be observed (Figure 3g).

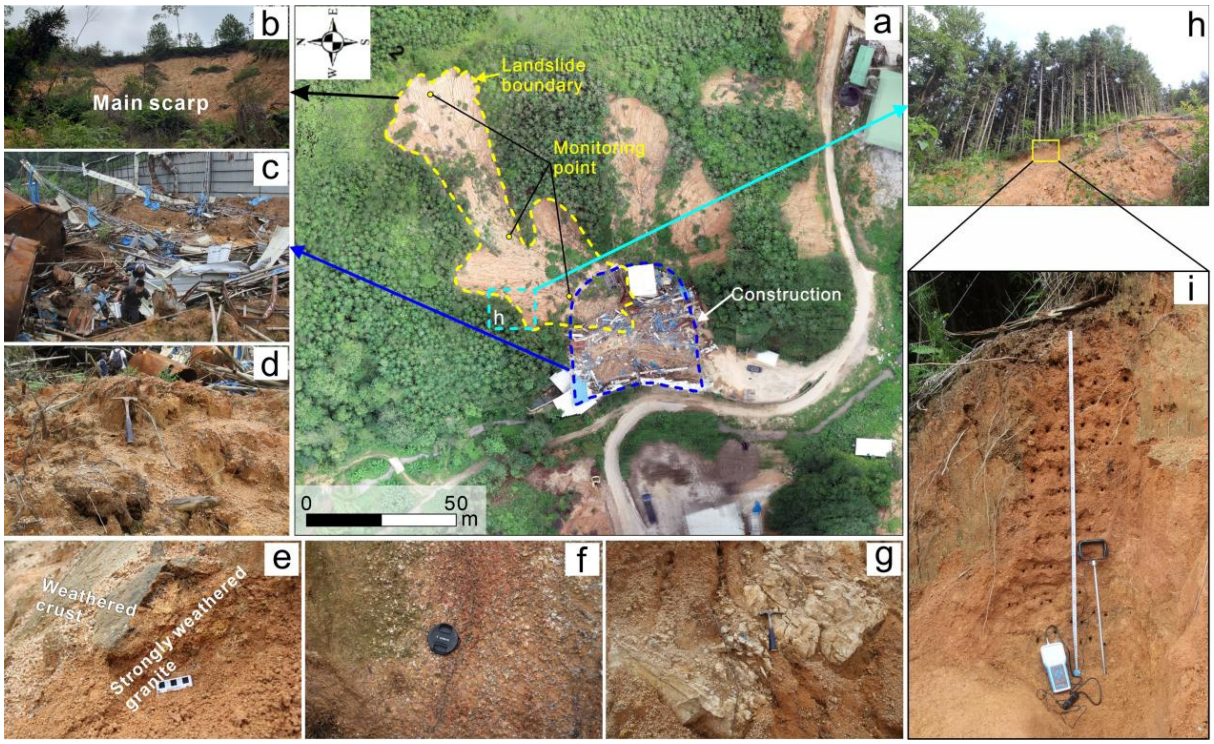


Figure 3. Panoramic plan view and typical photos indicating the details of the CT landslide. (**a**) Panoramic plan view. (**b**) Main scarp. (**c**) Destroyed constructions at the toe of the slope. (**d**) Exposed sliding surface. (**e**) Weathered crush of granite. (**f**) Sliding bed. (**g**) Cracked granite. (**h**) Location of trench. (**i**) Excavated trench.

To obtain the structure and soil composition of the Laifu landslide, a trench was excavated at the right flank (Figure 3i). The structural composition of the sliding mass was

revealed, and the sliding mass was divided into four layers (Figure 4). The top layer (L0) at a depth of 0~0.13 m is gray-black and red humus soil with a loose structure. The moisture of this layer is moderate, and the roots of vegetation are well developed. The second layer (L1) at a depth of 0.13~0.86 m comprises brown-red residual and deluvium soil with boulders inside. The soil around the boulders has low strength and is in an under-consolidated state. A small number of plant roots can be observed in the soil. The third layer (L2) at a depth of 0.86~1.19 m is composed of fully weathered granite. The quartz content of this layer is very high. The soil is slightly moist and has a dense structure. The bottom layer at a depth below 1.19 m (L3) is the strongly weathered granite with a clear original rock structure, and feldspar and mica have been weathered and altered. To determine the position of the sliding zone, the strength and moisture content of the sliding mass were measured by the in situ tests (hardness test and moisture content measurement) (Figure 4). The test results illustrate that the soil strength gradually increases and the volumetric moisture content decreases with an increase in depth above the interface between the strongly weathered granite and fully weathered granite. The soil strength tends to be stable, and the moisture content decreases rapidly and then stabilizes with an increase in depth below the interface between the strongly weathered granite and fully weathered granite. These facts demonstrate that the sliding zone is localized to the transitional interface between the strongly weathered granite and fully weathered granite. Moreover, a black weathering crust (of granite) with a thickness of 2~3 mm on the sliding surface was observed. Thus, it is further concluded that the Laifu landslide initiated at the weathering crust of granite mantled on the strongly weathered granite.

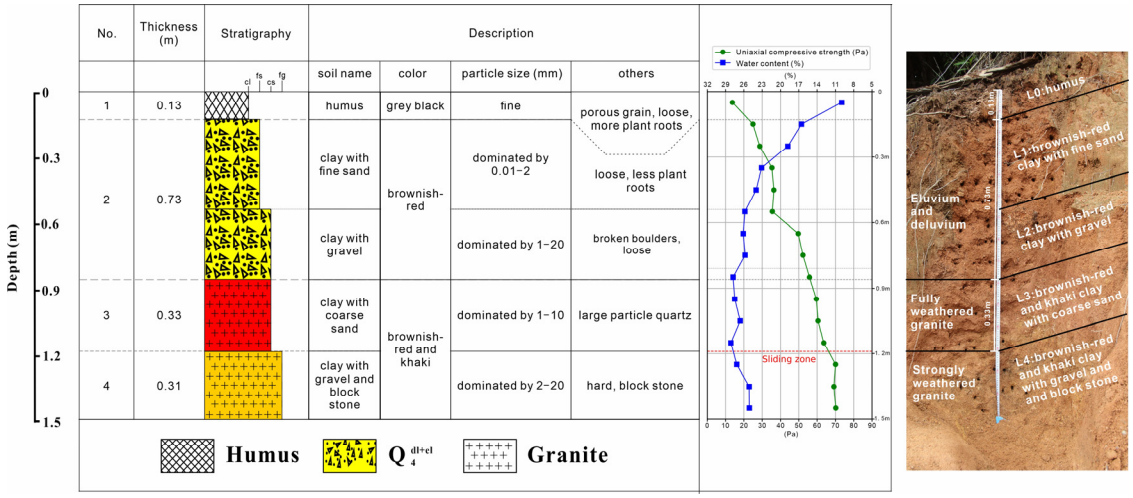


Figure 4. Representative stratigraphic section and soil geotechnical properties along the stratigraphic section at the crown of the Laifu landslide.

To obtain the post-failure Digital Elevation Model (DEM) and Digital Orthophoto Map (DOM), an Unmanned Aerial Vehicle (UAV, DJI Phantom 4 RTK) was used to conduct the onsite survey. Based on the post-failure DEM and onsite survey, the longitudinal profile of the Laifu landslide was depicted (Figure 5). The profile lines were denoted in the planar view (Figure 5). The mobilized apparent friction angle of the Laifu landslide is approximately 28.8°. The relatively short runout is a typical feature of rainfall-induced landslides in this region.

Field investigation revealed that the Laifu landslide occurred following a long period of rainfall. The surface soil mantled on the residual slope was saturated with rainwater and the soil weight increased accordingly. The sliding mass near both flanks and the main scarp converged into the central ravine, rapidly rushed downward, and accumulated at the foot of the slope. It is a typical channelized landslide featured with high speed and short runout.

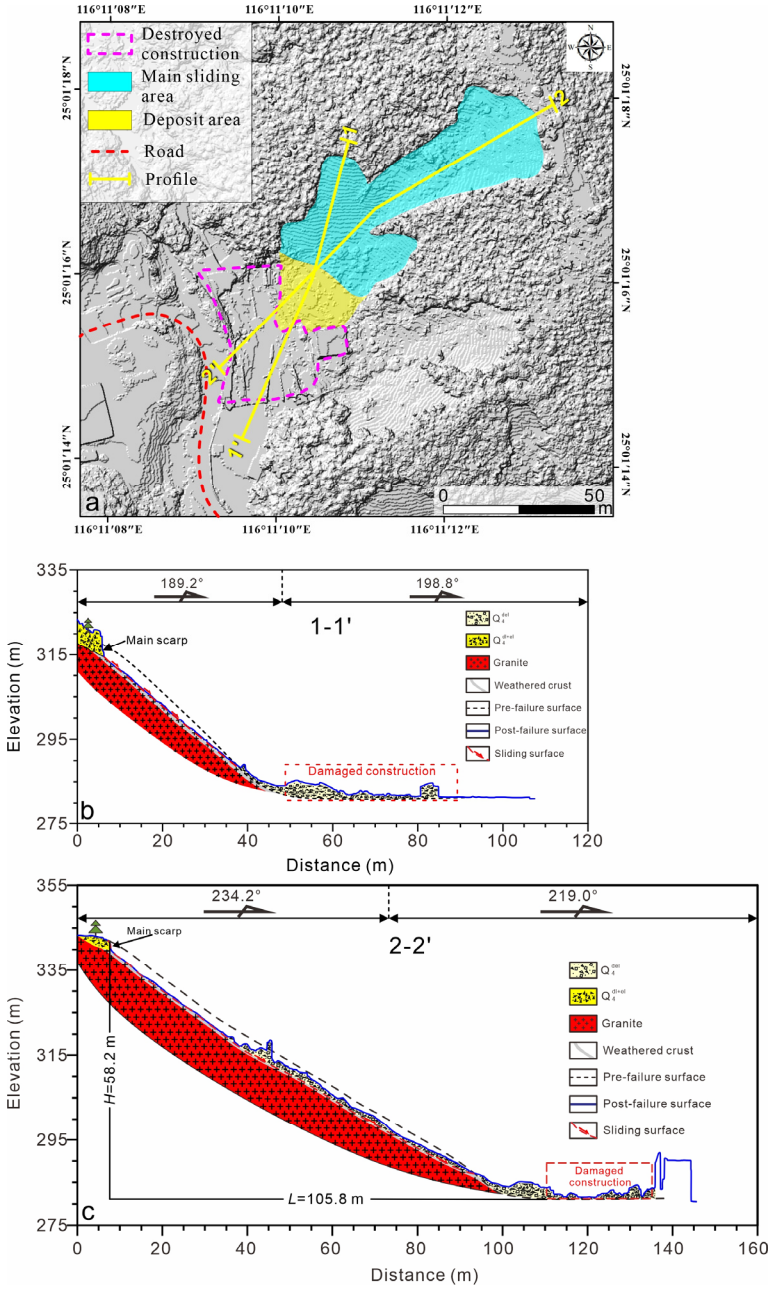


Figure 5. Planar view and longitudinal profiles of the Laifu landslide. (**a**) Planar view Planar of the Laifu landslide. (**b**) Longitudinal profile along line 1-1′. (**c**) Longitudinal profile along line 2-2′.

4. Triggering Factors

The study area is characterized by a typical subtropical monsoon climate with uneven monthly rainfall and the precipitation is mainly concentrated from April to September. Extreme precipitation is mostly recorded in this period. This region suffered intermittent heavy precipitation from 11 May 2022 to 27 May 2022 (landslide occurrence) and the cumulative rainfall during this period exceeded 400 mm. Moreover, the cumulative rainfall in Shifang Town, Wuping County from 6:00 a.m. on 24 May to 6:00 a.m. on 27 May reached 235.9 mm (Figure 6) and the maximum daily rainfall reached 206.4 mm from 6:00 on 26 May to 6:00 a.m. on 27 May. The 2 h rainfall in Shifang Town exceeded 120 mm from 23:00 on 26 May to 01:00 on 27 May and a maximum hourly rainfall of 56.0 mm was recorded. The extreme rainfall event in this region is rare in history. Moreover, the rainfall event was extremely uneven spatially. Figure 6 depicts the cumulative rainfall from 6:00 a.m. on 24

May to 6:00 a.m. on 27 May. It can be easily concluded that the severe convection weather was concentrated in the central area where landslides are densely distributed. Thus, it can be determined that the cascading landslides on 27 May 2022 were induced by the rain gush from the localized severe convection weather. The long-duration intermittent rainfall prior to this rainfall event may enhance the landslide occurrence.

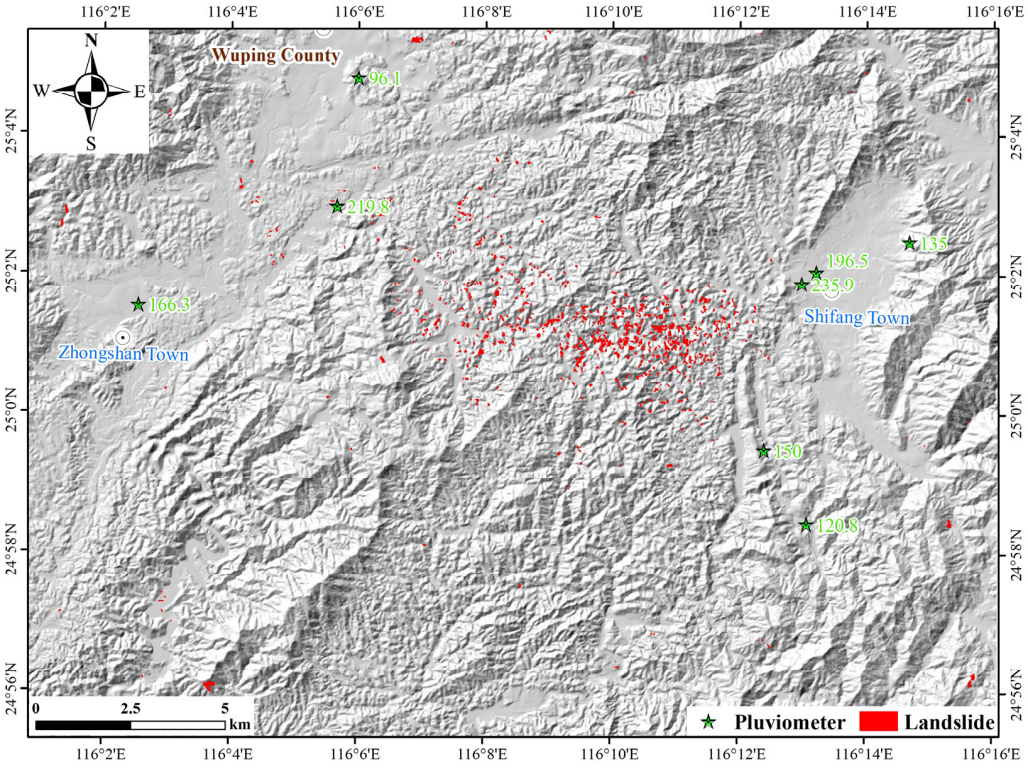


Figure 6. Distribution of landslides induced by the rain gush on 27 May 2022 and the cumulative precipitation from 7:00 a.m. on 24 May to 7:00 a.m. on 27 May.

The pre-failure terrain of the Laifu landslide area is gentle at the upper slope and steep at the lower slope. The relatively flat terrain of the upper slope provides a favorable condition for the convergence of overland flow, and precipitation can easily infiltrate into the slope along the cracks. It was discovered during the on-site investigation that the length (depth) of the vegetation roots on the slope was generally less than the thickness of the sliding mass. For slopes in Southeast China with a thick soil layer (>root depth), strong wind load and preferential flow resulting from root–soil interfaces, rather than slope surface infiltration, significantly decrease the slope stability in a short time [23]. This means the wind load exerted on the trees enhanced the development of cracks in the slope soil and the infiltration channels of overland flow could be enlarged in this process. The surficial soil of the shallow slope can be saturated rapidly during a rainstorm. Moreover, the upper soil layer of the slope mainly comprises loose residual soil, fully weathered granite, and strongly weathered granite with a dense structure and visible original rock structure. There is a significant difference in the permeability between the fully weathered granite and strongly weathered granite. The continuous infiltration of heavy rainfall resulted in the rapid accumulation of rainwater at the interface between the fully weathered granite and strongly weathered granite, increasing the weight of the soil and forming a weak sliding surface, which ultimately led to the occurrence of the catastrophic Laifu landslide. Long-term rainfall, the influence of vegetation roots under wind load, and differences in the strength and structure of surficial soil (rock) were the dominant factors for triggering cascading landslides in May 2022 in the study area.

5. Kinetic Analysis

5.1. Methodology

To explore the motion process of the catastrophic Laifu landslide, a Massflow platform was employed in this work. Massflow (v 2.0) is an efficient software for the dynamic process simulation of surface disasters and was developed based on the depth-integrated continuum model [28–30]. It employs a second-order solution of the depth integrated mass and momentum balance equations to obtain flow heights and velocities across a Cartesian grid inclined parallel to the pervading slope, modified to include the momentum exchange across the boundary layer due to entrainment [31]. In this work, the sliding mass is regarded as the continuous medium fluid in spatio-temporal calculations. Compared with previous discrete element numerical models, the calculation accuracy and efficiency are greatly improved, and the calculation time is shortened.

The physical friction models in Massflow software at present comprise the Coulomb model, Voellmy model, Manning model, etc. The Coulomb model has been widely used in motion simulation of landslide and debris flow in previous work [32–34]. The Coulomb model was selected as the base resistance model for the Laifu landslide in this work based on field investigation and previous cases. The key parameters involved in the kinetic analysis include mechanical parameters such as soil density (ρ), cohesion (c), mobility index (μ), and pore pressure ratio (λ). Based on our field investigation and previous research [4], the density and the cohesion of the sliding mass are set as 1.938 g/cm^3 and 13 kPa in the kinetic analysis. As indicated in the previous simulation, the internal friction angle has a limited impact on the motion feature of landslides, while the pore pressure ratio is the main factor affecting the travel distance and accumulation extent of landslides [35]. To investigate the most dangerous conditions under extreme rainstorms, the pore pressure ratio λ is set as 1. The mobility index of the Laifu landslide, defined as H/L (ratio of height to distance), was calculated to be 0.55 (Figure 5b). Key parameters of the Laifu landslide used in the numerical simulation are listed in Table 1.

Table 1. Key parameters of the Laifu landslide in the kinetic analysis.

Density of the Sliding Mass ρ (kg/m^3)	Cohesion (kPa)	Mobility Index μ	Pore Pressure Ratio λ
1938	13	0.55	1

To analyze the impact of the sliding mass on buildings under the most dangerous conditions, the sliding mass and the destroyed constructions at the foot of the slope were removed and set as a flat area. This ensured that the sliding mass could reach the location of the building with maximum impact without the energy loss that would result from the blockage of the construction at the foot of the slope. The calculation model with a grid number of 290 × 282 and a resolution of 0.5 m was constructed based on the UAV survey. The volume of the sliding mass was approximately 1600 m^3. The simulation results are highly consistent with the real case as the accumulation shape at the foot of the slope in the simulation matches the real case well (the shape of destroyed constructions).

5.2. Analysis of Kinematic Thickness and Velocity

To explore the characteristics of the Laifu landslide during its initiation, acceleration, and accumulation stages, the instantaneous thickness of the sliding mass during the motion and accumulation processes is depicted in Figure 7. Under the continuous infiltration of rainfall, a weak sliding surface was formed inside the slope and the whole slope became unstable in the first 1 s. In this process, the geopotential of the unstable sliding mass was transformed into kinetic energy. After the initiation of the Laifu landslide, the sliding mass of both sides converged to the central ravine at 1–2 s. Then, the sliding mass reached the edge of the buildings (factory) at the foot of the slope approximately within 3 s. The shape of the sliding mass is very consistent with the edge of the destroyed building,

indicating that the simulation results match the real motion of the Laifu landslide. During the downslope motion, the rear part was completely concentrated in the gully with a maximum thickness of more than 3 m at 4–5 s. The sliding mass moved downward at a high speed along the gully and further impacted the buildings again, which led to serious casualties and damage to buildings at 5–6.4 s. The thickness of the sliding mass directly affects the disaster intensity. The thickness of the Laifu landslide before its motion was approximately 0.5~1.5 m. Affected by the terrain of the central gully, the maximum thickness of the landslide can reach 5.03 m, which greatly enhances the disaster intensity of landslides. Therefore, it can be concluded that the catastrophic effect of channelized shallow landslides is more severe than that of hillslope shallow landslides induced by typhoons and rainstorms.

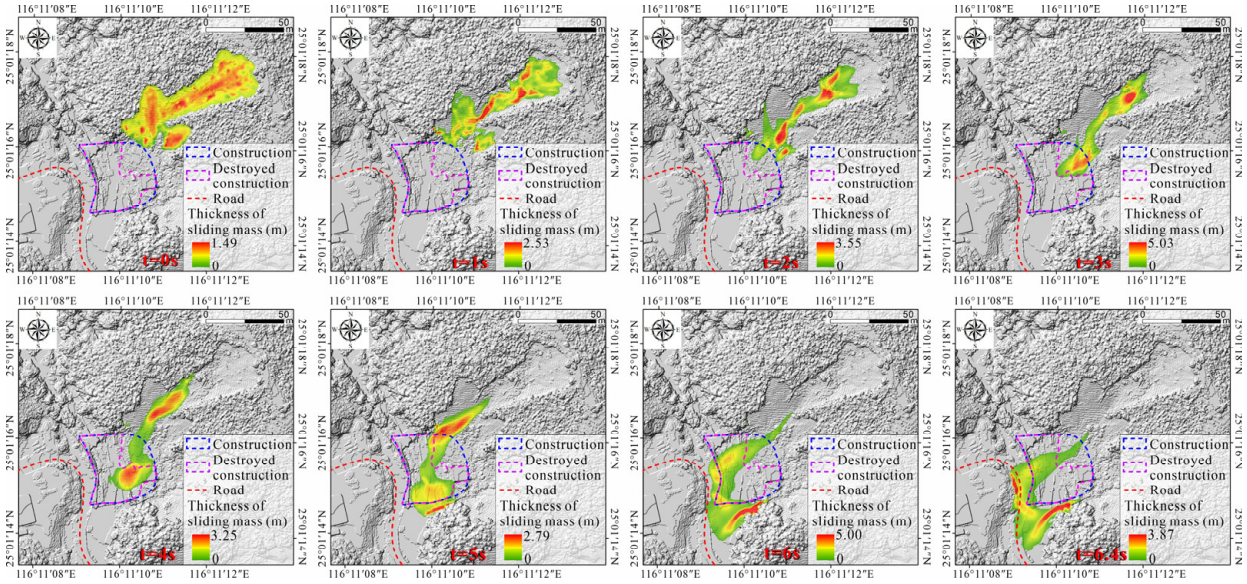


Figure 7. Thickness distribution of sliding mass of the Laifu landslide at different time.

Investigation of the kinematic velocity of landslides is an important part of disaster reduction and prevention, and the kinematic velocity and runout are deemed to be restricted by the terrain conditions [36]. The spatial distribution of the kinematic velocity of the Laifu landslide at each moment is depicted in Figure 8. The results show that the Laifu landslide is a channelized landslide, and its kinematic velocity is significantly affected by the gully. The middle and lower parts of the sliding mass accelerated continuously during the movement of the sliding mass. At t = 3 s, the sliding mass reached the edge of the destroyed building and reached a maximum speed of about 22 m/s. The maximum speed of the following sliding mass was about 29 m/s when it reached the destroyed building. It should be noted that the kinematic velocity of the Laifu landslide suffered a decrease when it arrived at the central valley. The decrease in velocity is attributed to the gentle terrain of both banks of the valley and the sharp terrain of the central valley. The central valley resulted in the energy loss of the sliding mass and a portion of the sliding mass rested in the valley. The majority of the sliding mass converged in the central valley and rushed along the valley again. This part of the sliding mass received energy supply from the following mass and the velocity increased gradually then. The characteristics of landslide kinematic velocity indicated that changes in terrain slope and gully shape are key factors that cannot be ignored for channelized landslides. The combined effect of terrain and gully shape can significantly affect the disaster intensity of channelized landslides.

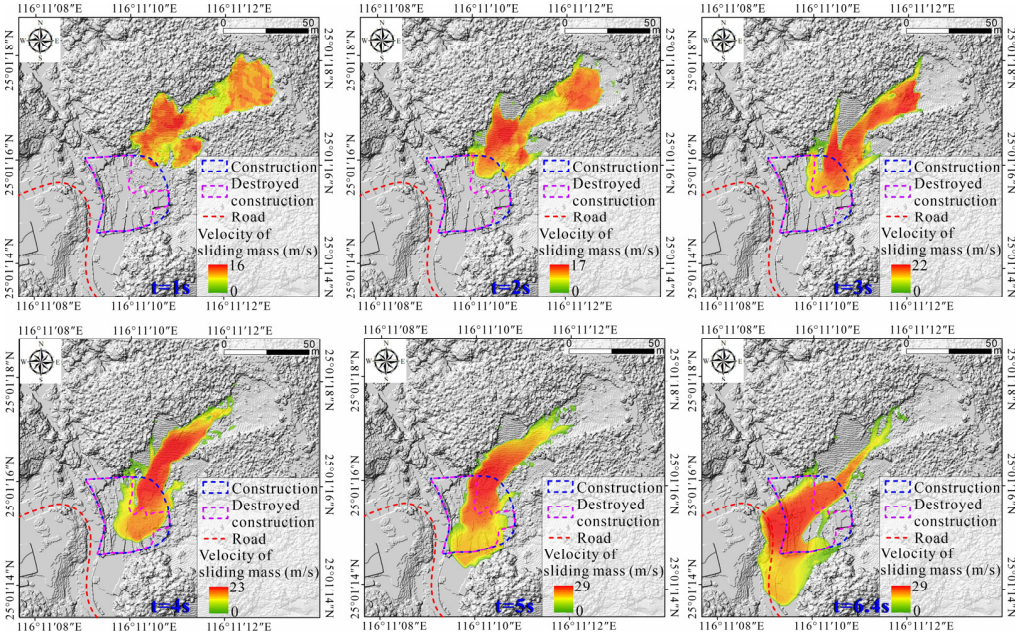


Figure 8. Velocity distribution of the sliding mass of the Laifu landslide at different times.

5.3. Analysis of Impact Energy and Force

The disaster intensity can be directly reflected by the impact energy and impact force on buildings. The impact energy of the sliding mass is determined by the thickness of the sliding mass and its kinematic velocity. The kinetic energy of each grid during the movement of the sliding mass was calculated based on the thickness and kinematic velocity of the Laifu landslide. This work was conducted based on the programming in the Massflow platform, and the value of hv^2 (h is the thickness and v is the kinematic velocity of each grid) was calculated at first. Then, the calculated data were exported to the ArcGIS platform and the kinetic energy (Figure 9) was calculated as the multiplication hv^2, g (gravitational acceleration), and A (the area of each grid) with the raster calculator tool in the ArcGIS. In the first 3 s, the sliding mass in the middle and lower part of the Laifu landslide completely rushed down. The first impact of the sliding mass on the building at the foot of the slope appeared at this stage, and the maximum impact energy was approximately 2834.65 J. Then, the second impact occurred after the upper sliding mass crossed the narrow gully in the middle of the landslide and rushed downward to the building in 3–6.4 s, with a maximum impact energy of 4221.35 J.

The aforementioned analysis presents the temporal features of the Laifu landslide at different times. To further explore the kinetic features of the Laifu landslide at different locations, three monitoring points were set to record the temporal change in thickness, velocity, and impact energy of the sliding mass at fixed locations. Points 1, 2, and 3 are located at the boundary of the building before it was destroyed, the middle slope, and the upper slope (Figure 3a). The numerical simulation indicates that it only took 0.5 s for the Laifu landslide to travel from its initiation to its initial deposition at point 1. At this stage, the lower part of the sliding mass reached the construction area first with low kinetic velocity (Figure 10a), and a limited impact on the building was expected. From 1.8 s, the velocity and thickness of monitoring point 3 stayed stable, which means nearly all sliding mass from the source area slid down and converged into the gully. At 3 s, the velocity of monitoring point 1 reached the first peak, and the middle and lower parts of the sliding mass completely moved down and reached the building. The velocity of monitoring point 2 is characterized by a steep decline, confirming the influence of gully geometry (shape) and terrain changes on the landslide motion velocity (Figure 10b). The relation between velocity and time shows that the velocities of monitoring point 1 and point 2 were 29 m/s and 22 m/s, respectively (Figure 10b). The thicknesses of monitoring point 1 and point 2 were

2.8 m and 1.6 m, respectively (Figure 10a). The velocities and thicknesses of monitoring point 1 and point 2 remained nearly unchanged after 6.4 s. It is speculated that the building (factory) at the foot of the slope was buried by the Laifu landslide within 6.4 s from the initiation. Thus, there was not enough time to avoid the landslide impact.

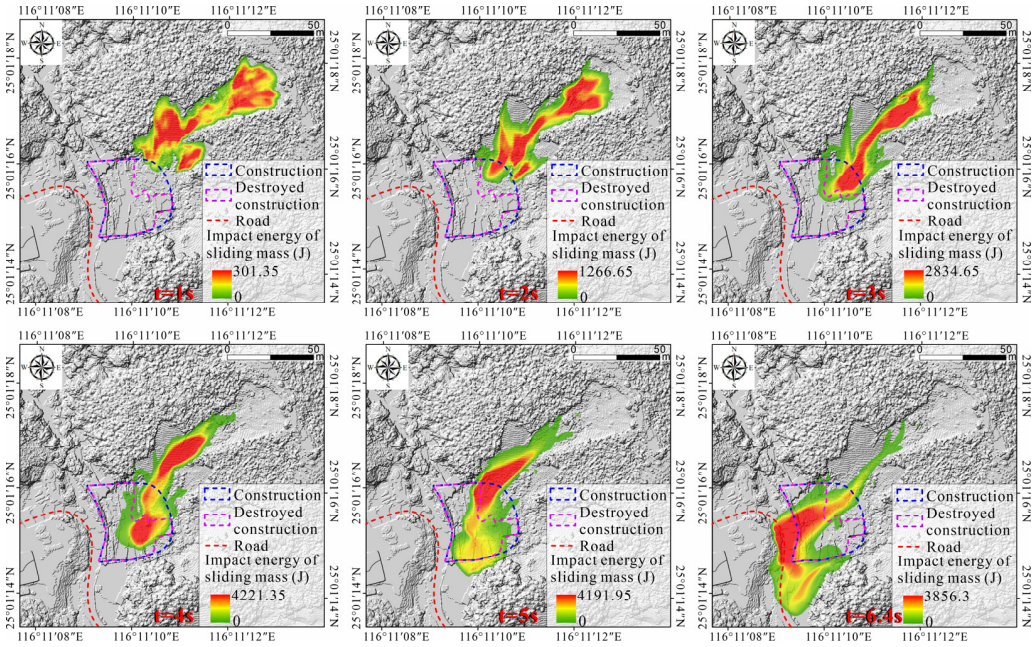


Figure 9. Impact energy distribution of the sliding mass of the Laifu landslide at different times.

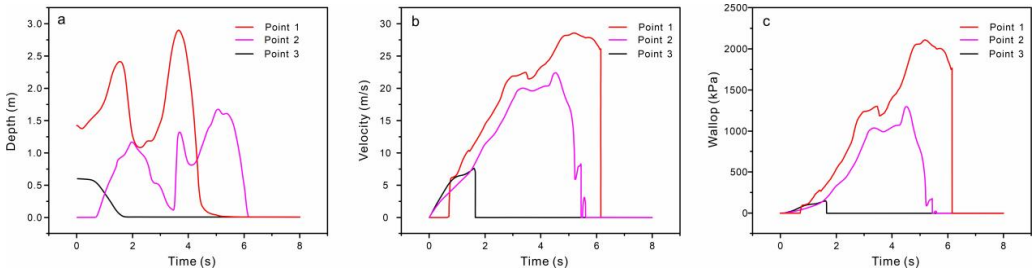


Figure 10. Relation between kinetic features (thickness, velocity, and impact force) and time at three monitoring points of the Laifu landslide. (**a**) Relation between thickness and time at three monitoring points. (**b**) Relation between velocity and time at three monitoring points. (**c**) Relation between impact force and time at three monitoring points.

In addition to impact energy, impact force is another key factor reflecting the damage of landslides to constructions. At present, the calculation model for the impact force of landslides remains immature. An empirical equation (Equation (1)) based on the kinetic velocity and thickness of the sliding mass was used to estimate the impact force on the building in this work [37,38].

$$\delta = \varepsilon \frac{\gamma_c}{g} V_c^2 sin\alpha \quad (1)$$

where δ is the impact force (kPa) and ε is the coefficient indicating the shape or configuration of constructions. This value is set as 1 when the construction is round, while the values of 1.33 and 1.47 will be selected when the constructions are rectangular and square. α is the intersection angle between the thrust surface and the direction of impact force.

Based on our field investigation, ε is determined to be 1.33 and α is set as 90° in the Laifu case. The impact force of three monitoring points was calculated and depicted in Figure 10c. Generally, a building is deemed to be damaged when the maximum impact force is higher than 100 kPa [39]. It can be spotted from the evolution of the impact force that

the value of the impact force continued to increase to a peak value of 2110 kPa within 5 s and the buildings were destroyed and buried in this period. This value is much greater than the threshold of impact force for construction damage. Thus, it is preliminarily concluded that it is difficult for residential buildings in mountainous areas to withstand the impact of (even shallow) landslides induced by rainfall.

6. Conclusions

Based on a comprehensive investigation including UAV surveys, trench observations, in situ tests, and kinetic analyses, the types and spatial distribution of cascading landslides triggered by heavy rainfall on 27 May 2022 in Wuping were investigated. More than 700 landslides were induced in this event, with their general sliding direction consistently aligning with the slope aspect, indicating a clear relationship between the topography and the landslide occurrence. The cascading landslides were primarily controlled by extreme rainfall associated with severe convection weather patterns, which underscored the critical role of meteorological conditions in landslide initiation. The spatial distribution of these landslides closely matched the patterns of cumulative rainfall, providing a clear correlation between rainfall intensity and landslide occurrence. This relationship highlights the need for effective monitoring of weather conditions to anticipate and mitigate landslide risks.

Several factors contributed to the triggering of these cascading landslides, including long-term rainfall, the structural influence of vegetation roots under wind load, and variations in the strength and structure of the surficial soil. The region's geology featured a relatively uniform slope structure and soil composition, characterized by a sliding mass comprised of gray-black and red humus soil with a loose structure, brown-red residual and deluvium soil containing boulders, and fully weathered granite. The sliding surface was localized at a depth of 1–1.5 m, specifically at the interface between fully weathered and strongly weathered granite, as determined by in situ tests and field investigations.

Landslides in the 2022 Wuping event were primarily classified into two categories: channelized and hillslope types. They were characterized by short runout distances and high mobility, particularly among the channelized landslides. These landslides demonstrated significant impact energy and force, which were attributed to the convergence of the sliding mass in the central valley. This convergence intensified the kinetic energy of the landslides, making constructions situated at the toe of the slopes particularly vulnerable to catastrophic impact failure. The mobilized apparent friction angle of the channelized Laifu landslide, measured at approximately 28.8°, further illustrates the conditions contributing to the landslides' dynamics. The short runout, a typical feature of rainfall-induced landslides in this region, exacerbates the risk to infrastructure and human safety.

The channelized landslide in the 2022 Wuping event was particularly notable for its rapid velocity and the sheer force of its movement. The numerical analysis illustrates that the channelized landslide (which resulted in severe casualties) is characterized by the maximum values of 29 m/s for velocity, 4221.35 J for impact energy, and 2110 kPa for impact force. This immense kinetic energy had severe consequences, as the construction at the foot of the slope was rapidly buried within just 5 s due to the powerful impact of the sliding mass. The abrupt occurrence of the landslide events posed significant challenges for timely evacuation from the potential impact zone, underscoring the urgent need for improved disaster preparedness and response strategies in areas prone to such geological hazards.

The occurrence of mass geological disasters triggered by extreme rainfall in southeastern coastal China is critical, emphasizing the urgent need for rainfall-type dynamic analysis. This work focuses on massive geological disasters triggered by extreme rainfall in 2022, specifically identifying typical pre-failure slope structures and susceptible layers in the region. The dynamic analysis primarily addressed the dynamic evolution and runout process of typical rainfall-induced landslides under the most extreme (and dangerous) conditions. However, the study did not investigate how rainfall patterns affect infiltration and the mechanisms through which this infiltration leads to slope instability. This aspect is

a significant component of landslides induced by extreme rainfall in residual accumulative layers. Furthermore, considering the effects of wind load and plant root systems on slope instability is a critical issue that requires attention from us and other researchers.

Author Contributions: T.W., R.L. and C.C. drafted the manuscript; T.W., J.H., C.Z., S.Z., L.Y. and K.L. conducted the field investigation; J.H. and K.N. conducted the simulation and risk assessment. All authors have read and agreed to the published version of the manuscript.

Funding: This work was financially supported by the Key Laboratory of Geohazard Prevention of Hilly Mountains, Ministry of Land and Resources (Fujian Key Laboratory of Geohazard Prevention) (KLGHZ202103), the Ministry of Natural Resources, People's Republic of China (121106000000180039-2207), the China Geological Survey (DD20221738), the National Natural Science Foundation of China (42207234 and 42302333), and the Fundamental Science Foundation of Institute of Geomechanics (DZLXJK202007).

Data Availability Statement: The data presented in this study are all available on request.

Acknowledgments: The authors are grateful for the endeavor devoted by the editor and reviewers; their useful comments and advice are highly appreciated.

Conflicts of Interest: The authors declare no conflicts of interest.

References

1. Ying, M.; Wan, R. The annual frequency prediction of tropical cyclones affecting China. *J. Appl. Meteor. Sci.* **2011**, *22*, 66–76.
2. Yu, H.; Hu, C.; Jiang, L. Comparison of three tropical cyclone intensity datasets. *J. Meteorol.* **2007**, *21*, 121–128.
3. Ren, R.; Yu, D.; Wang, L.; Wang, K.; Wang, H.; He, S. Typhoon triggered operation tunnel debris flow disaster in coastal areas of SE China. *Geomat. Nat. Hazards Risk* **2019**, *10*, 562–575. [CrossRef]
4. Yan, J.; Huang, J.; Li, H.; Chen, H.; Chen, L.; Zhang, Y. Study on instability mechanism of shallow landslide caused by typhoon and heavy rain. *J. Geomech.* **2020**, *26*, 481–491.
5. Liang, X.; Segoni, S.; Yin, K.; Du, J.; Chai, B.; Tofani, V.; Casagli, N. Characteristics of landslides and debris flows triggered by extreme rainfall in Daoshi Town during the 2019 Typhoon Lekima, Zhejiang Province, China. *Landslides* **2022**, *19*, 1735–1749. [CrossRef]
6. Yu, B.; Chen, W.; Feng, W.; Liu, K.; Ye, L. A case study of shallow landslides triggered by rainfall in Sanming, Fujian Province, China. *Environ. Earth Sci.* **2023**, *82*, 426. [CrossRef]
7. Wang, J.; Gong, Q.; Yuan, S.; Chen, J. Combining soil macropore flow with formation mechanism to the development of shallow landslide warning threshold in South China. *Front. Earth Sci.* **2023**, *10*, 1048427. [CrossRef]
8. Huang, F.; Xiong, H.; Jiang, S.H.; Yao, C.; Fan, X.; Catani, F.; Chang, Z.; Zhou, X.; Huang, J.; Liu, K. Modelling landslide susceptibility prediction: A review and construction of semi-supervised imbalanced theory. *Earth Sci. Rev.* **2024**, *250*, 104700. [CrossRef]
9. Huang, F.; Teng, Z.; Yao, C.; Jiang, S.H.; Catani, F.; Chen, W.; Huang, J. Uncertainties of landslide susceptibility prediction: Influences of random errors in landslide conditioning factors and errors reduction by low pass filter method. *J. Rock. Mech. Geotech. Eng.* **2024**, *16*, 213–230. [CrossRef]
10. Chang, Z.; Huang, F.; Huang, J.; Jiang, S.H.; Liu, Y.; Meena, S.R.; Catani, F. An updating of landslide susceptibility prediction from the perspective of space and time. *Geosci. Front.* **2023**, *14*, 101619. [CrossRef]
11. Huang, F.; Mao, D.; Jiang, S.H.; Zhou, C.; Fan, X.; Zeng, Z.; Catani, F.; Yu, C.; Chang, Z.; Huang, J.; et al. Uncertainties in landslide susceptibility prediction modeling: A review on the incompleteness of landslide inventory and its influence rules. *Geosci. Front.* **2024**, *15*, 101886. [CrossRef]
12. Huang, F.; Li, R.; Catani, F.; Zhou, X.; Zeng, Z.; Huang, J. Uncertainties in landslide susceptibility prediction: Influence rule of different levels of errors in landslide spatial position. *J. Rock. Mech. Geotech. Eng.* 2024, *in press*. [CrossRef]
13. Zhang, J.; Tang, H.; Li, C.; Gong, W.; Zhou, B.; Zhang, Y. Deformation stage division and early warning of landslides based on the statistical characteristics of landslide kinematic features. *Landslides* **2024**, *21*, 717–735. [CrossRef]
14. Fang, K.; Tang, H.; Li, C.; Su, X.; An, P.; Sun, S. Centrifuge modelling of landslides and landslide hazard mitigation: A review. *Geosci. Front.* **2023**, *14*, 101493. [CrossRef]
15. Wen, T.; Tang, H.; Wang, Y.; Lin, C.; Xiong, C. Landslide displacement prediction using the GA-LSSVM model and time series analysis: A case study of Three Gorges Reservoir, China. *Nat. Hazards Earth Syst. Sci.* **2017**, *17*, 2181–2198. [CrossRef]
16. Zhang, J.; Tang, H.; Tannant, D.D.; Lin, C.; Xia, D.; Liu, X.; Zhang, Y.; Ma, J. Combined forecasting model with CEEMD-LCSS reconstruction and the ABC-SVR method for landslide displacement prediction. *J. Clean. Prod.* **2021**, *293*, 126205. [CrossRef]
17. Wen, T.; Tang, H.; Huang, L.; Wang, Y.; Ma, J. Energy evolution: A new perspective on the failure mechanism of purplish-red mudstones from the Three Gorges Reservoir area, China. *Eng. Geol.* **2020**, *264*, 105350. [CrossRef]
18. Fang, K.; Miao, M.; Tang, H.; Jia, S.; Dong, A.; An, P.; Zhang, B. Insights into the deformation and failure characteristic of a slope due to excavation through multi-field monitoring: A model test. *Acta Geotech.* **2023**, *18*, 1001–1024. [CrossRef]

19. Lin, Q.; Steger, S.; Pittore, M.; Zhang, J.; Wang, L.; Jiang, T.; Wang, Y. Evaluation of potential changes in landslide susceptibility and landslide occurrence frequency in China under climate change. *Sci. Total Environ.* **2022**, *850*, 158049. [CrossRef]
20. Li, Z.; Zhang, F.; Gu, W.; Dong, M. The Niushou landslide in Nanjing City, Jiangsu Province of China: A slow-moving landslide triggered by rainfall. *Landslides* **2020**, *17*, 2603–2617. [CrossRef]
21. Greco, R.; Marino, P.; Bogaard, T.A. Recent advancements of landslide hydrology. *Wiley Interdisciplinary Reviews: Water* **2023**, *10*, e1675. [CrossRef]
22. Sun, C.; Tang, C.; Cheng, Q.; Xu, J.; Zhang, D. Stability of Soil Slope under Soil-Atmosphere Interaction. *Earth Sci.* **2022**, *47*, 3701–3722.
23. Zhuang, Y.; Xing, A.; Petley, D.; Jiang, Y.; Sun, Q.; Bilal, M.; Yan, J. Elucidating the impacts of trees on landslide initiation throughout a typhoon: Preferential infiltration, wind load and root reinforcement. *Earth Surf. Process. Landf.* **2023**, *48*, 3128–3141. [CrossRef]
24. Chen, F.; Jia, H.; Du, E.; Wang, L.; Wang, N.; Yang, A. Spatiotemporal variations and risk analysis of Chinese typhoon disasters. *Sustainability* **2021**, *13*, 2278. [CrossRef]
25. Luo, Y.; Yang, M.; Ni, P.; Peng, X.; Yuan, X. Degradation of rammed earth under wind-driven rain: The case of Fujian Tulou, China. *Constr. Build. Mater.* **2020**, *261*, 119989. [CrossRef]
26. Yu, S.; Ren, X.; Zhang, J.; Wang, H.; Sun, Z. An improved form of smoothed particle hydrodynamics method for crack propagation simulation applied in rock mechanics. *Int. J. Min. Sci. Techno* **2021**, *31*, 421–428. [CrossRef]
27. Su, Z.; Wang, Y.; Zhang, H. Study on the Failure Mechanism, Safety Grading and Rainfall Threshold of Landslide Caused by Typhoon Rainstorm. *Geotech.* **2022**, *40*, 2201–2211. [CrossRef]
28. Ouyang, C.; He, S.; Xu, Q.; Luo, Y.; Zhang, W. A MacCormack-TVD finite difference method to simulate the mass flow in mountainous terrain with variable computational domain. *Comput. Geosci.* **2013**, *52*, 1–10. [CrossRef]
29. Ouyang, C.; He, S.; Xu, Q. MacCormack-TVD Finite Difference Solution for Dam Break Hydraulics over Erodible Sediment Beds. *J. Hydraul. Eng.* **2015**, *141*, 06014026. [CrossRef]
30. Ouyang, C.; An, H.; Zhou, S.; Wang, Z.; Su, P.; Wang, D.; Cheng, D.; She, J. Insights from the failure and dynamic characteristics of two sequential landslides at Baige village along the Jinsha River, China. *Landslides* **2021**, *16*, 1397–1414. [CrossRef]
31. Tai, Y.; Kuo, C. A new model of granular flows over general topography with erosion and deposition. *Acta Mech.* **2008**, *199*, 71–96. [CrossRef]
32. Ouyang, C.; Zhou, K.; Xu, Q.; Yin, J.; Peng, D.; Wang, D.; Li, W. Dynamic analysis and numerical modeling of the 2015 catastrophic landslide of the construction waste landfill at Guangming, Shenzhen, China. *Landslides* **2017**, *14*, 705–718. [CrossRef]
33. Zhou, K. *Numerical Simulation of Disaster Dynamics Based on Single-Layer Single-Phase Flow and Multilayer Multi-Phase Flow*; Huazhong University of Science and Technology: Wuhan, China, 2017.
34. Yang, H.; Cheng, Q.; He, J.; Xing, B.; Xiao, S. First insights into a debris avalanche blocking the Tonghua No. 1 tunnel in China's Sichuan-Tibet traffic corridor on 5 July 2022. *Landslides* **2023**, *20*, 865–870. [CrossRef]
35. Zhou, Q.; Xu, Q.; Zhou, S.; Peng, D.L.; Zhou, X.P.; Qi, X. Movement Process of Abrupt Loess Flowslide Based on Numerical Simulation-A Case Study of Chenjia 8# on the Heifengtai Terrace. *J. Mt. Sci.* **2019**, *37*, 528–537.
36. Li, X.; Fu, H.; Zhang, Y.; Xiao, X.; Dong, Y.; Xiang, C. Study on the Influence of Topography on Landslide Mobility. *J. Disaster Prev. Mitig.* **2020**, *40*, 867–877.
37. Ding, B. Bridge Risk Assessment under Tailings Dam Failure Hazard with GIS and Massflow Simulation. Master's Thesis, Huazhong University of Science and Technology, Wuhan, China, 2019.
38. Mei, T.; Xiao, S.X. Mechanism analysis of bridge piers damaged by debris flow. *Shanxi Archit.* **2021**, *37*, 151–152.
39. Dong, Y.; Ren, J.; Zhou, L. Risk assessment method based on landslide dynamic process simulation: A case study of Sinan landslide in Guizhou Province. *Gansu Water Resour. Hydropower Technol.* **2019**, *55*, 26–34.

Disclaimer/Publisher's Note: The statements, opinions and data contained in all publications are solely those of the individual author(s) and contributor(s) and not of MDPI and/or the editor(s). MDPI and/or the editor(s) disclaim responsibility for any injury to people or property resulting from any ideas, methods, instructions or products referred to in the content.